Development 121, 1989-2003 (1995)
Printed in Great Britain © The Company of Biologists Limited 1995

The role of *Hoxa-3* in mouse thymus and thyroid development

Nancy R. Manley and Mario R. Capecchi*

Howard Hughes Medical Institute, Department of Human Genetics, University of Utah School of Medicine, Salt Lake City, Utah 84112, USA

*Author for correspondence

SUMMARY

Targeted disruption of *Hoxa-3* results in a number of regionally restricted defects in tissues and structures derived from or patterned by mesenchymal neural crest. However, analysis of mutant embryos with injections of a carbocyanine dye or with molecular markers that label these cells indicates that neither the amount nor the migration patterns of this neural crest population are grossly affected. Therefore, it appears that the loss of *Hoxa-3* affects the intrinsic capacity of this neural crest cell population to differentiate and/or to induce proper differentiation of the surrounding pharyngeal arch and pouch tissues. *Hoxa-3* mutant mice are athymic and show thyroid hypoplasia. Thymus development is first evident as an expansion of mesenchymal neural crest in the posterior part of the 3rd pharyngeal pouch. Prior to this expansion, a marked reduction in *pax-1* expression is observed in these cells in the mutant embryos. As *pax-1* mutant mice also show thymic hypoplasia, these results suggest that *Hoxa-3* may be required to maintain *pax-1* expression in these cells and that the reduction of *pax-1* expression is part of the athymic teleology in *Hoxa-3* mutant mice. The thyroid gland is formed from the fusion of two structures of separate embryonic origin, the thyroid diverticulum, which is formed from endodermal epithelium in the floor of the pharynx, and the ultimobranchial body, formed from mesenchymal neural crest in the 4th pharyngeal pouch. Both of these sites express *Hoxa-3* and are defective in mutant mice. Often a vesicle is observed in mutant mice that is exclusively composed of calcitonin-producing cells, suggesting the persistence of an ultimobranchial body. Both aspects of the thyroid phenotype show variable expressivity among mutant animals, even on the two sides of the same mutant animal. This variability suggests the presence of a compensating gene or genes, whose utilization is stochastic. A reasonable candidate for providing this compensatory function is the paralogous gene *Hoxb-3*.

Key words: *Hox* genes, homeobox genes, *Hoxa-3*, neural crest, *pax-1*, mouse development, thymus, thyroid, DiGeorge syndrome

INTRODUCTION

The pharyngeal arches and pouches are transient embryonic structures that give rise to many of the tissues and organs in the head and neck region of vertebrates. The cranial neural crest arising from the embryonic midbrain and hindbrain plays a critical role in the development of the pharyngeal arches and pouches, initially by providing the mesenchymal cells which populate this region. As development proceeds, the neural crest mesenchyme contributes directly to the formation of some structures in this region (e.g. cartilage, connective tissue, glandular derivatives), and also patterns other tissues through inductive interactions (LeLievre and LeDouarin, 1975; Noden, 1983, 1988; Hall, 1981, 1987; Bockman and Kirby, 1984). Transplantation experiments in the chick suggest that prior to leaving the neural tube, the neural crest cells are prepatterned to contribute to structures appropriate to their axial level of origin (Noden, 1983).

One group of genes implicated in regulating the development of the pharyngeal region is the family of *Hox* genes (Hunt et al., 1991a, b). These genes encode a class of transcription factors that contain a highly conserved DNA binding motif, the *Antennapedia* homeodomain (Kissinger et al., 1990; Otting et al., 1990). Humans and mice contain 38 *Hox* genes distributed in four linkage groups (designated as Hox A, Hox B, Hox C and Hox D) on four separate chromosomes. Based on DNA sequence similarity, individual members of the four linkage groups have been classified into 13 paralogous families (Scott, 1992).

Members of the four most 3′ paralogous families have the most rostral limits of expression in the developing hindbrain, with cranial expression boundaries spaced at approximately two segment (i.e. rhombomere) intervals (Fig. 1A). In addition to their expression domains in the neural tube, these *Hox* gene transcripts are also found in neural crest cells prior to, during, and subsequent to their migration into the pharyngeal arches. For example, the *Hoxb-2* gene is expressed in the neural tube up to the boundary between rhombomeres 2 and 3 (r2/r3), in neural crest migrating from r4 and posterior, and in the pharyngeal arches 2, 3 and 4 (Wilkinson, 1989; Hunt, 1991a, b). The *Hoxb-3* gene, located immediately 5′ of *Hoxb-2*, has a cranial limit of expression in the developing hindbrain at r4/r5, and is expressed in the neural crest emanating from r6 and posterior and in the 3rd and 4th pharyngeal arches (Sham et

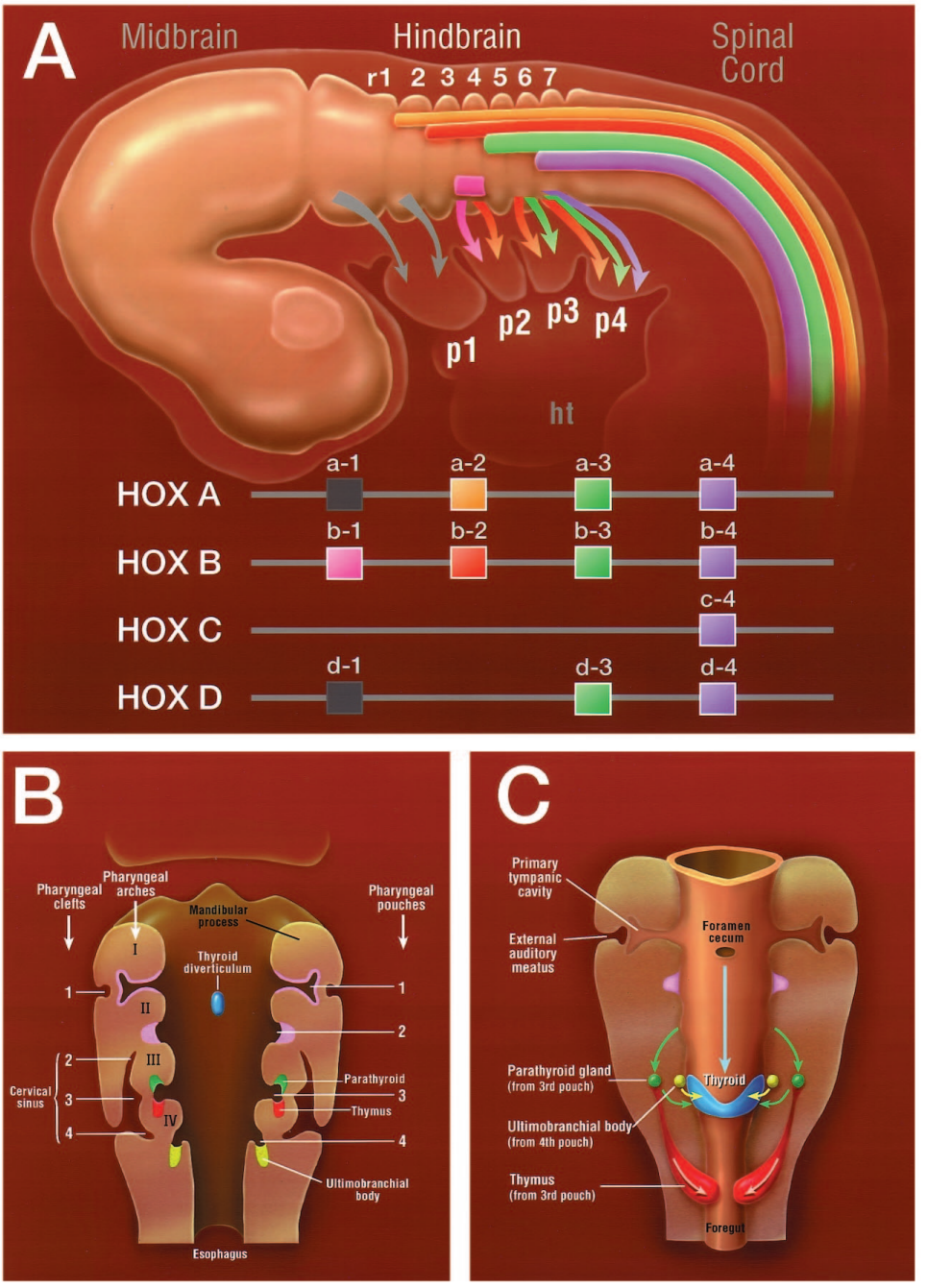

Fig. 1. (A) Schematic diagram of *Hox* gene expression in the hindbrain and pharyngeal region at E9.5. Colored bars within the neural tube and colored arrows correspond to the expression domains of paralogous groups of *Hox* genes. The genes represented in the diagram are indicated in the same colors at the bottom of A. Arrows represent expression in neural crest cells which migrate into the pharyngeal arches according to their axial level of origin. In the first paralogous family, only *Hoxb-1* is expressed in the hindbrain and neural crest at this stage. In the second paralogous group, *Hoxa-2* has its cranial expression limit in rhombomere 2 (r2), but is not expressed in the neural crest migrating from r2. Neural crest originating in r1 and r2 express no *Hox* genes. r, rhombomere; p, pharyngeal arch; ht, heart. (B) Coronal section through the pharyngeal arch region at E11. The second arch is beginning to overgrow the third and fourth arches, resulting in the formation of the cervical sinus by the 2nd, 3rd, and 4th clefts. Pouch derivatives are beginning to form, as indicated on the right side of the diagram. The thymus is beginning to form from the posterior half of the third pharyngeal pouch. The two structures that will contribute to the mature thyroid gland are the thyroid diverticulum, forming from the ventral surface of the pharynx, and the ultimobranchial body, forming from the fourth pharyngeal pouch. Colors in B and C do not correspond to colors used in A. (C) Ventral view of the pharyngeal organ derivatives. Structures are shown in the same colors as their sites of origin shown in B. The thyroid gland forms from the posterior migration of the thyroid diverticulum from the ventral floor of the pharynx and the medial and ventral migration of the ultimobranchial bodies, which fuse to form the mature thyroid gland. The foramen cecum is an opening formed by the outpocketing and migration of the thyroid diverticulum, which closes later in development. The parathyroids from the third pouch migrate to a variable position which is generally lateral to the thyroid gland. The two thymic primordia, also from the third pouch, migrate medially and posteriorly, where the two structures fuse to become a single gland ventral to the trachea. The tympanic cavity and external auditory meatus are formed from the first pharyngeal pouch and cleft, respectively.

al., 1992). This spectrum of gene expression suggests that *Hox* genes convey patterning information from the hindbrain into the target pharyngeal arches via the migrating neural crest (Hunt et al., 1991a, b). It is of further interest that the ectodermal and endodermal epithelial cells of the pharyngeal arches and pouches also express subsets of the *Hox* genes. It is not known whether *Hox* gene expression in these cell layers arises as a consequence of interaction with the incoming mesenchymal neural crest or is achieved independently of this interaction.

Mice with targeted disruptions in *Hoxa-1*, *Hoxa-2* and *Hoxa-3* all have defects in tissues derived from or patterned by neural crest. Thus, *Hoxa-1* mutant mice, in addition to their neural tube defects, also have deficiencies in cranial ganglia derived from neural crest (Lufkin et al., 1991; Chisaka et al., 1992; Carpenter et al., 1993; Dollé et al., 1993; Mark et al., 1993). *Hoxa-2* mutant mice have defects in the neural crest-derived middle ear ossicles, which were interpreted as a change of identity in these elements (Gendron-Maguire et al., 1993; Rijli et al., 1993). *Hoxa-3* mutants have a spectrum of abnor-

malities in the pharyngeal tissues derived from or patterned by mesenchymal neural crest, particularly those arising from the 3rd and 4th pharyngeal arches. These defects include deletions and malformations of the throat cartilages and bones of the jaw, disorganization of the throat musculature, of the heart and great vessels, deletions of the thymus and parathyroids, and thyroid hypoplasia (Chisaka and Capecchi, 1991).

This paper presents experiments undertaken to examine the developmental origins of the *Hoxa-3* mutant phenotype. We demonstrate that in the absence of *Hoxa-3*, neither the amount nor the migration pattern of mesenchymal neural crest appears to be grossly affected, suggesting that the absence of *Hoxa-3* gene product may affect instead the intrinsic capacity of this neural crest cell population to differentiate and/or to induce proper differentiation of surrounding tissues. The defects in the thymus and thyroid glands of *Hoxa-3* mutant mice provided a way to investigate this possibility. Both of these structures originate in the pharyngeal arches and pouches (Fig. 1B,C) and have a large neural crest contribution to their development (LeLievre and LeDouarin, 1975; Noden, 1983, 1988; Bockman and Kirby, 1984). In addition, formation of both glands depends on interactions with other cell types, notably the pharyngeal endoderm (Auerbach, 1960; Hilfer, 1968; Cordier and Haumont, 1980; Bockman and Kirby, 1984). We show that in *Hoxa-3*⁻ mutants the thymus defect is evident early in development, and may involve down regulation of *pax-1*. The thyroid defect, however, does not result from the deletion of either of its two major cell types, the endodermally derived follicular cells or the neural crest derived parafollicular cells. Instead, both cell types are reduced in number and do not interact with each other normally. In many cases, the tissues derived from these two cell types fail to fuse and develop instead as separate structures.

MATERIALS AND METHODS

Generation of mice and genotyping

Mice heterozygous for a targeted disruption of the *Hoxa-3* gene were intercrossed to produce embryos of all three possible genotypes. The mutant allele contained an insertion of the MC1neopA cassette within sequences encoding the third helix of the homeodomain (Chisaka and Capecchi, 1991). Embryonic age was estimated by considering noon of the day of a vaginal plug as E0.5. Embryos used in whole-mount in situ hybridization or immunofluorescence analysis were age matched to within 2 somites.

Mice were genotyped by either Southern blot or PCR analysis of yolk sac or tail DNA. Southern blots were performed as previously described (Chisaka and Capecchi, 1991). PCR analysis was performed in 30 μl reactions amplified for 32-35 cycles with 1 minute at 94°C, 30 seconds at 60°C, 1 minute plus 1 second per cycle at 72°C. The *Hoxa-3*-specific PCR primers were located at the intron/exon boundary 5′ of the homeobox (5′ primer), and 340 bases 3′ of the site of the *neo*ʳ cassette insertion in the homeobox. The *neo* primer was located at the 3′ end of the MC1neopA cassette. The sequences of primers used were: 5′ primer, 5′-TCTTCCTCTCTGTGTCCTG-GCAG-3′; 3′ primer, 5′-ATAGCTGCCATTGCCCTGCAG-3′; neo primer, 5′-TCTATCGCCTTCTTGACGAGTTC-3′. PCR products were analyzed using polyacrylamide gel electrophoresis.

Dye injection and embryo culture

Dye injection of embryos and embryo culture were performed essentially as previously described (Serbedzija et al., 1992). E8.5 embryos obtained from intercrosses of *Hoxa-3* heterozygotes were dissected from the decidua in 20% fetal bovine serum (FBS)/80% high glucose Dulbecco's modified Eagle's medium (DMEM), leaving the extraembryonic membranes intact. After equilibrating for 1 hour at 37°C in embryo culture medium (50% DMEM/25% rat serum/25% FBS with 250 Units/ml penicillin, 0.25 mg/ml streptomycin), a small amount of DiI was injected into the amniotic cavity using a backfilled micropipette and a picospritzer. DiI was made as a 0.5% stock solution in 100% ethanol and diluted 1:10 in 0.3 M sucrose at 37°C immediately before use.

Embryos were cultured in pairs overnight in 2 ml embryo culture medium in an atmosphere of 5% CO_2 in air at 37°C in an embryo culture roller apparatus (BTC Engineering). After 20-24 hours in culture, embryos were dissected from the placenta and extraembryonic membranes and fixed in 4% formaldehyde in phosphate-buffered saline (PBS) overnight at 4°C. Genotypes were determined by PCR analysis of the yolk sac DNA. Embryos were then rinsed in PBS and cleared in 90% glycerol in PBS. Cleared embryos were mounted in depression slides and viewed in whole mount through a rhodamine filter set using a laser scanning BioRad MRC600 confocal microscope and COMOS software. Serial optical sections were pseudo-colored and compiled into a Z series image.

Whole-mount in situ hybridization and sectioning

Whole-mount in situ hybridizations were performed essentially as described by Carpenter et al. (1993). E9.5-E11 mouse embryos were fixed overnight in 4% formaldehyde in PBS, then dehydrated in methanol and stored at −20°C until use. The digoxigenin-labelled RNA probes were used at 0.5 μg/ml. Alkaline phosphatase-conjugated anti-digoxigenin Fab fragments were used at 1:5000. Color reactions were carried out over time periods ranging from 2 hours to overnight. Embryos were photographed without clearing, with Ektachrome 160T film using a Wild dissecting microscope.

The following probes were used for whole-mount in situ hybridization. The *Hoxa-2* probe was a 338 base pair *Apa*I-*Eco*RV fragment from the coding region 3′ of the homeobox. The *Hoxa-3* probe was a 650 base pair *Eco*RI cDNA fragment containing the first coding exon and the homeobox; the *b-3s* transcript was detected using a 500 base pair sense strand transcript from a *Hoxb-3* cDNA which spans the *Hoxb-3* stop codon; the *fgf-3* probe was a 373 base pair *Pst*I-*Eco*RI cDNA fragment beginning 152 base pairs 5′ of the stop codon. Two *pax-1* probes were used, both generously provided by Rudi Balling. One probe was a 313 base pair *Hin*cII-*Sac*I fragment containing the *pax-1* paired box (Deutch et al., 1988). The second probe was an 800 base pair cDNA fragment from a *Bsp*EI site to the stop codon, containing the entire coding sequence except for the paired box. Both probes gave the same results.

Embryos stained in whole mount were processed for sectioning by standard paraffin embedding. Embryos were sectioned at 8 or 10 μm, counterstained with Nuclear Fast Red (Mansour et al., 1993), and mounted in DPX. Sections were photographed in bright-field illumination using didymium and neutral density filters with Ektachrome 64T film on a Leitz Ortholux microscope.

Generation of a *Hoxb-1*-specific antibody and immunofluorescence

The *Hoxb-1* polyclonal antibody was generated as described by Wall et al. (1992). A fusion protein that contains the majority of the first exon of *Hoxb-1* (*Eag*I-*Hpa*II 417 base pair fragment, 139 amino acids) and the glutathione-S-transferase gene (GST, Smith and Johnson, 1988), was produced in *E. coli* and purified by adsorption to GST-Sepharose beads. Purified fusion protein was injected into rabbits using a 750 μg initial lymph node injection with 750 μg intramuscular boosts, by the Berkeley Antibody Company (BAbCo). Antibodies against the Hoxb-1 protein were affinity purified using the Hoxb-1-GST fusion protein after subtraction of antibodies against GST and bacterial proteins. Absence of antibodies to GST was confirmed by western blot.

For immunofluorescence and detection of *Hoxb-1*, E9.5 embryos were fixed overnight in 4% formaldehyde, washed in phosphate-buffered saline with 1% Tween-20 (PBST), dehydrated, and stored in 100% methanol. After rehydration, embryos were washed 3 times for 60 minutes in PBS, then blocked in PBS/5% donkey serum/1% Triton X-100 at room temperature (RT). Primary antibody incubation was performed using a 1:200 dilution in blocking solution for 3 days at 4°C. Embryos were washed 3×60 minutes in PBS/1% donkey serum/1% Triton X-100 at RT. FITC-conjugated donkey-anti-rabbit secondary antibody (Jackson ImmunoResearch) was diluted 1:400 in PBS/1% donkey serum/1% Triton X-100 and incubated overnight at 4°C. After 3×60 minute washes, embryos were refixed for 15 minutes in 4% formaldehyde, washed again in PBS, and cleared in 90% glycerol. Cleared embryos were mounted in depression slides and examined and photographed using a BioRad MRC600 confocal microscope and COMOS software. Serial optical sections were compiled into a Z series image. The images shown in Fig. 6 were processed with a 5×5 median filter. Pseudocolor was added to enhance contrast, with red as the most intense fluorescence and blue as the least.

Immunohistochemistry

Immunolocalization of the CRABP1 protein was performed essentially as described by Wall et al. (1992) using an antibody generously provided by U. Eriksson (Eriksson et al., 1987). Embryos were fixed in 4% formaldehyde and stored in methanol as described above. After rehydration, embryos were treated with hydrogen peroxide, washed, and blocked in PBS/10% FBS/1%Triton X-100 and incubated with the CRABP1 antibody at 1:300 dilution in blocking solution overnight at 4°C. Embryos were washed in blocking solution, and incubated with a donkey anti-rabbit 2° antibody conjugated to horseradish peroxidase at 1:500 dilution overnight. After washing again, the signal was visualized with diaminobenzidine. After the color reaction, the embryos were refixed in 4% formaldehyde in PBS, and stored in PBS at 4°C. Photography was performed as described for whole-mount in situ hybridizations.

Calcitonin immunohistochemistry was performed using a polyclonal antibody against human calcitonin (ICN) which cross-reacts with the mouse product. Newborn animals were killed by CO_2 asphyxiation, fixed in Bouins solution for up to 1 week or in 4% formaldehyde in phosphate-buffered saline overnight at room temperature and embedded in paraffin. 10 or 12 μm serial sections were collected and processed for immunostaining using a horseradish peroxidase-conjugated secondary antibody essentially as described (Wall et al., 1992; Gamer and Wright, 1993). Endogenous peroxidases were inhibited by a 30 minute incubation in methanol/0.6% H_2O_2. Sections were blocked for 20 minutes in 10 mM Tris pH 7.4, 100 mM $MgCl_2$, 0.5% Tween 20, 1% BSA, and 5% fetal bovine serum. Primary antibody incubation was performed for 1 hour using a 1:200 dilution in TBST (10 mM Tris pH 8.0, 150 mM NaCl, 0.05% Tween 20). Sections were washed 2×10 minutes in TBST. The donkey anti-rabbit secondary antibody was diluted 1:1000 in TBST and incubated for 30 minutes. After washing in TBST, color reactions were developed using 0.6 mg/ml diaminobenzidine and 0.06% H_2O_2 in PBS. Color reactions were performed for 15 minutes. Sections were counterstained with Nuclear Fast Red (Mansour et al., 1993), and mounted in DPX. Sections were photographed in bright-field illumination using a didymium filter with Ektachrome 64T film on a Leitz Ortholux microscope.

RESULTS

Defects in pharyngeal arch 2-derived structures are not the result of effects on *Hoxa-2* expression

Hoxa-3 mutant mice have defects in structures and tissues derived from pharyngeal arch 2, whereas the rostral limit of *Hoxa-3* expression in the pharyngeal region is arch 3 (Fig. 2). Since *Hoxa-2* is expressed in the 2nd pharyngeal arch (Hunt et al., 1991a; Tan et al., 1992), and mutations in *Hoxa-2* result, in part, in the deletion of skeletal elements derived from the 2nd arch (Gendron-Maguire et al., 1993; Rijli et al., 1993), it was possible that the presence of the *neo*^{r} cassette in the homeodomain of *Hoxa-3* might affect the expression of *Hoxa-2*. In order to test this possibility, the expression of *Hoxa-2* was examined in *Hoxa-3* mutant embryos.

Fig. 3 shows the expression of *Hoxa-2* in E9.5 and E10.5 wild-type and *Hoxa-3* mutant embryos. *Hoxa-2* expression is observed in the neural tube caudal to the r1/r2 boundary, in neural crest emanating from r4, and in the 2nd pharyngeal arch. No alterations in the expression pattern of *Hoxa-2* in *Hoxa-3* mutant embryos were detected. In particular, *Hoxa-2* expression

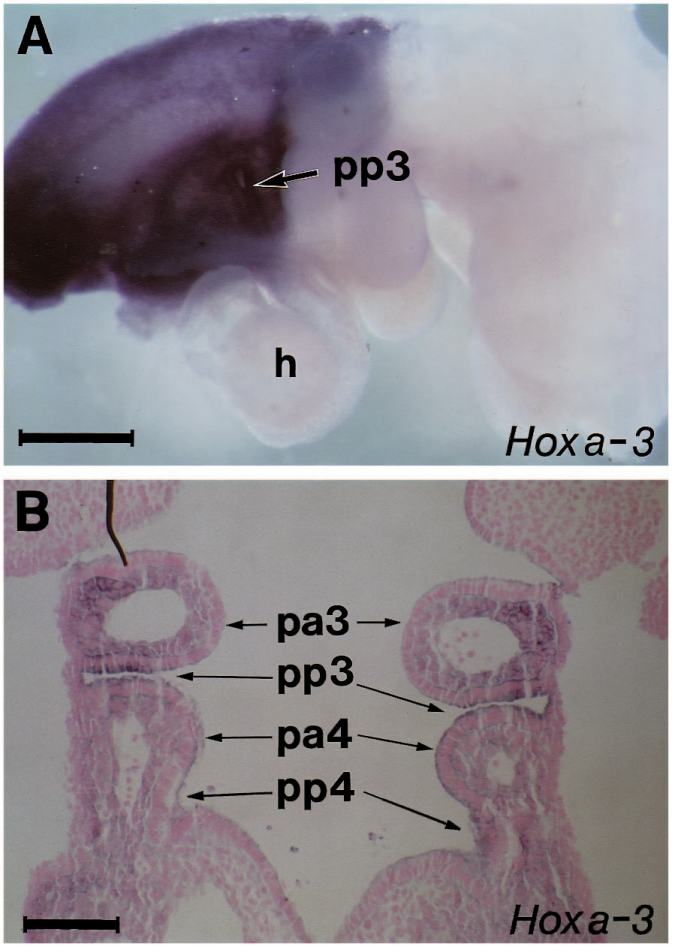

Fig. 2. Expression of the *Hoxa-3* gene in the pharyngeal arches at E10.5. (A) Whole-mount in situ hybridization analysis of an E10.5 embryo. Dorsal is up, cranial is to the right. The cranial limit of expression of *Hoxa-3* is at the r4/r5 boundary in the neural tube, and at the level of the 3rd pharyngeal arch in the branchial region. Expression in the 3rd pharyngeal pouch is indicated by the arrow (pp3). (B) 8 μm coronal section through the same E10.5 embryo shown in A. Cranial is up. *Hoxa-3* expression is seen in the mesenchyme throughout the third and fourth arches (pa3, pa4), as well as in the endodermal epithelial cells of the third and fourth pouches (pp3, pp4). pa, pharyngeal arch; pp, pharyngeal pouch; h, heart. Scale bars, (A) 400 μm; (B) 100 μm.

in the neural crest migrating from rhombomere 4 into the 2nd pharyngeal arch at E9.5 and the characteristic pattern of *Hoxa-2* expression in the 2nd pharyngeal arch at E10.5 appear unchanged. *Hoxa-2* expression in *Hoxa-3* mutants was also observed to be indistinguishable from that in wild-type at 8.5 days of gestation (data not shown). These results indicate that the most cranial aspects of the *Hoxa-3* mutant phenotype are not the result of secondary effects on *Hoxa-2* expression.

Neural crest migration appears normal in *Hoxa-3* mutants

Many of the structures and tissues affected in *Hoxa-3* mutant mice have their embryological origins in the pharyngeal arches and pouches. Neural crest ablation and transplantation experiments in the chick, as well as analysis of chick/quail chimeras, have shown that these structures and tissues are derived from or patterned by neural crest which originates in the midbrain and hindbrain region and migrates into the pharyngeal arches (LeLievre and LeDouarin, 1975; Bockman and Kirby, 1984; Noden, 1983, 1988). It is possible that part or all of the *Hoxa-3* mutant phenotype could be caused by an alteration in migration or a reduction in this neural crest population. To test this possibility, cranial neural crest was examined in *Hoxa-3* mutant embryos using two methods, DiI labelling of premigratory neural crest in culture, and molecular marking of this cell population.

Injection of the lipophilic dye DiI into the amniotic cavity of an embryo has been shown to label cells on the surface of the embryo, including premigratory neural crest cells in the neural tube where the neural tube has not yet closed (Serbedzija et al., 1992). After incubation in culture, the migration of labelled neural crest cells can be followed using confocal microscopy. Embryos from *Hoxa-3* intercrosses were dissected at E8.5, leaving the yolk sac and placenta intact. DiI was injected into the amniotic sac, and the embryos were allowed to develop for 20-26 hours in culture. After culture, the embryos were inspected and normally developing embryos were examined by confocal microscopy. Fig. 4 shows heterozygous (A) and mutant embryos (B) in which labelled neural crest can be seen emigrating from r4 into arch 2. Fig.

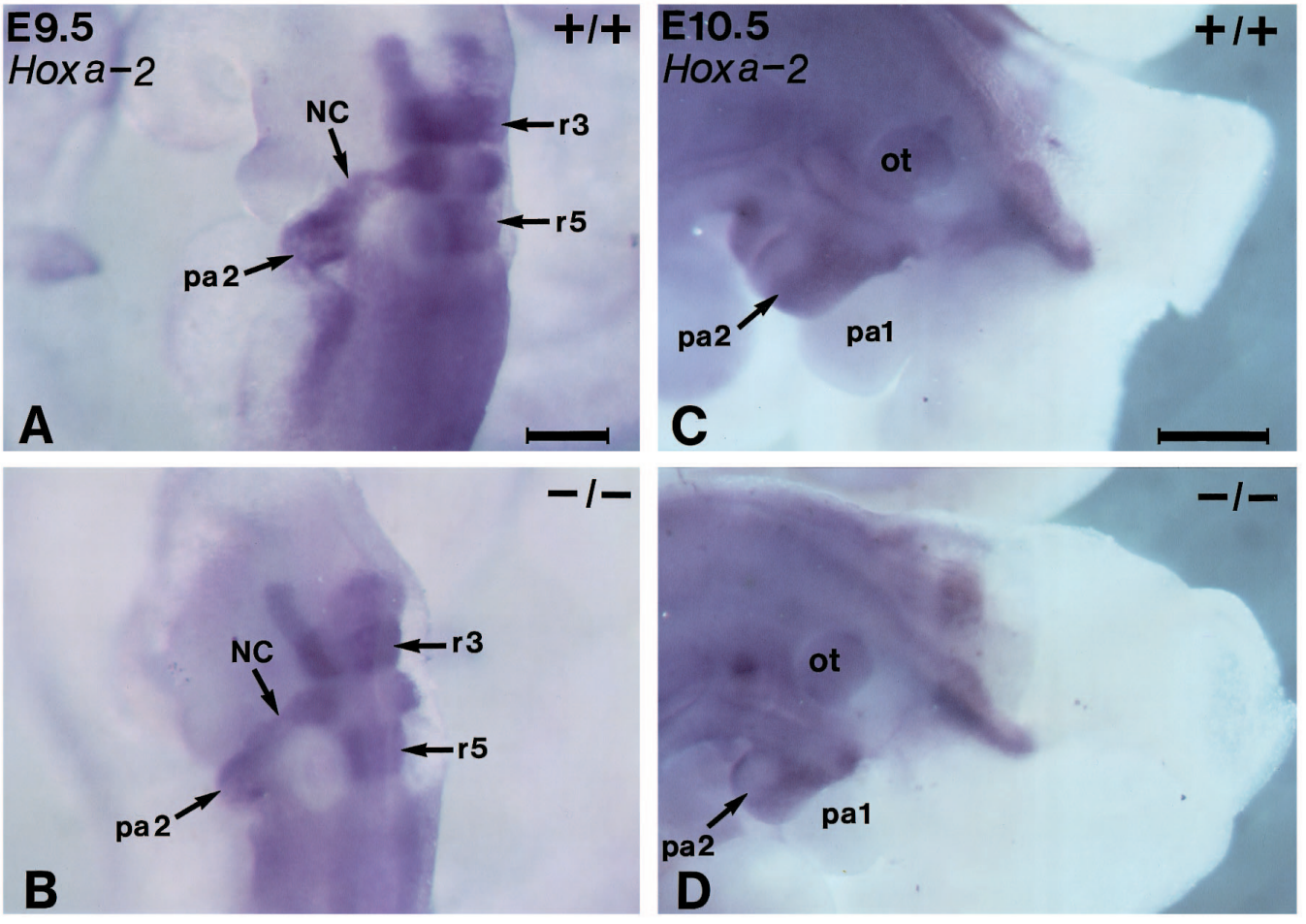

Fig. 3. The expression of *Hoxa-2* in E9.5 and E10.5 control and *Hoxa-3* mutant embryos. All embryos are stained by whole-mount in situ hybridization for *Hoxa-2* expression. (A) Dorsolateral view of an E9.5 wild-type embryo. Cranial is up. *Hoxa-2* expression is seen in the rhombomeres, migrating neural crest (NC), and pharyngeal arch 2 (pa2). (B) Similar view of a *Hoxa-3*$^{-/-}$ embryo. Differences in the *Hoxa-2* expression pattern in *Hoxa-3* wild-type and mutant embryos are not apparent. (C) Dorsolateral view of an E10.5 wild-type embryo. Cranial is to the right. Note the stronger signal in the rostral half of the second pharyngeal arch (pa2). (D) Similar view of a *Hoxa-3*$^{-/-}$ embryo. This *Hoxa-2* expression is not distinguishable from the wild-type embryonic pattern; note the pattern of staining in pa2. r, rhombomere; NC, neural crest; pa, pharyngeal arch; ot, otocyst. Scale bar, (A,B) 200 μm; (C,D) 400 μm.

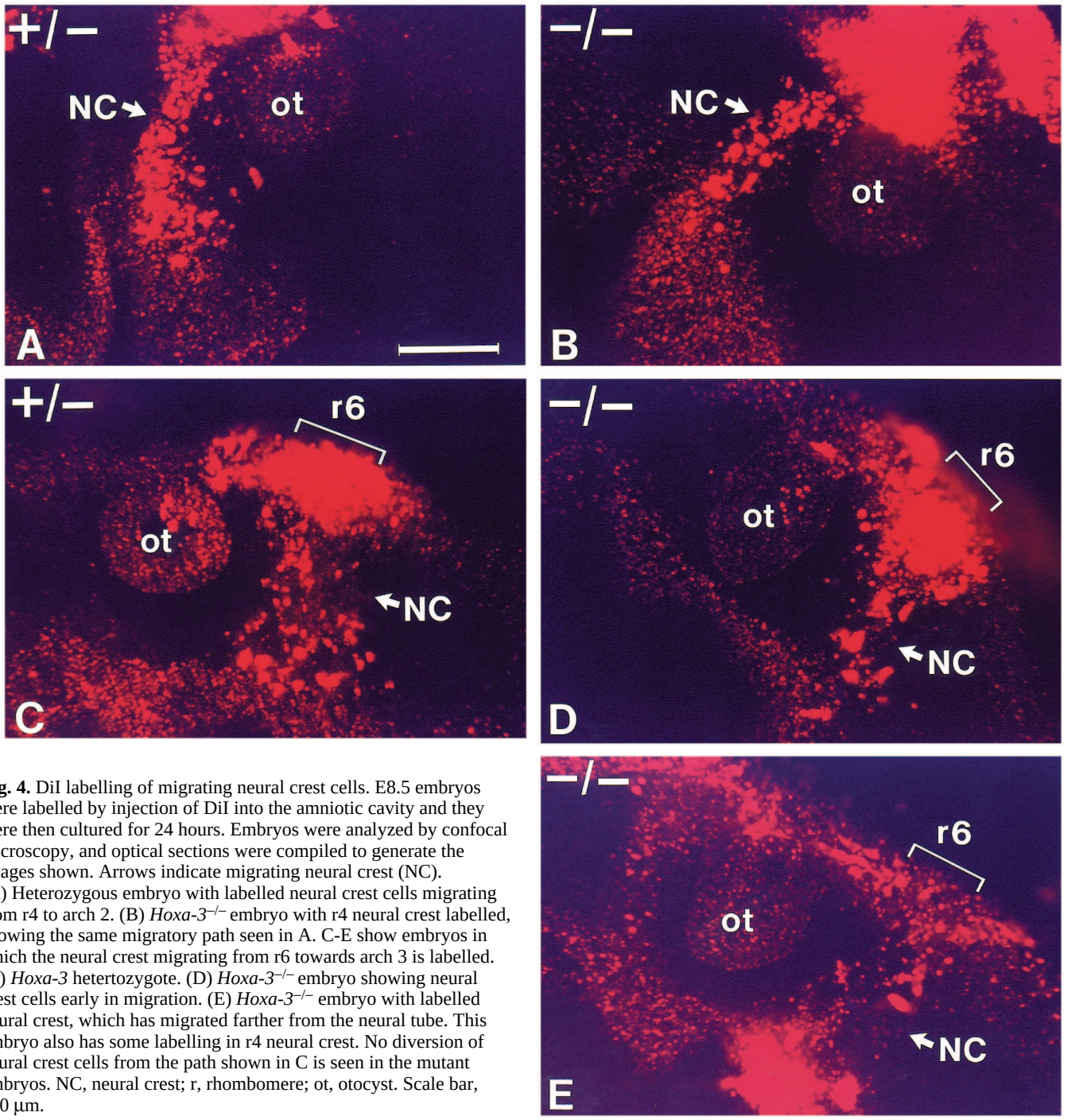

Fig. 4. DiI labelling of migrating neural crest cells. E8.5 embryos were labelled by injection of DiI into the amniotic cavity and they were then cultured for 24 hours. Embryos were analyzed by confocal microscopy, and optical sections were compiled to generate the images shown. Arrows indicate migrating neural crest (NC). (A) Heterozygous embryo with labelled neural crest cells migrating from r4 to arch 2. (B) *Hoxa-3*$^{-/-}$ embryo with r4 neural crest labelled, showing the same migratory path seen in A. C-E show embryos in which the neural crest migrating from r6 towards arch 3 is labelled. (C) *Hoxa-3* hetertozygote. (D) *Hoxa-3*$^{-/-}$ embryo showing neural crest cells early in migration. (E) *Hoxa-3*$^{-/-}$ embryo with labelled neural crest, which has migrated farther from the neural tube. This embryo also has some labelling in r4 neural crest. No diversion of neural crest cells from the path shown in C is seen in the mutant embryos. NC, neural crest; r, rhombomere; ot, otocyst. Scale bar, 150 μm.

4C-E show a control and two mutant embryos with labelled neural crest cells migrating from r6 into arch 3. The labelled cells of the mutant embryo in D are at an earlier stage of migration than those of the mutant embryo in E. Although the extent of migration of labelled cells varied from embryo to embryo, no consistent differences between mutant and control embryos were seen, either in the number of cells or in their migration pattern. All labelled cells emanating from a given rhombomere migrated along the same general path, with no diversions of subsets of labelled cells to other targets.

The marker gene analysis was performed using several molecular markers that have been shown previously to label neural crest cells in the hindbrain region. An antibody against the CRABP1 protein was used to label E9.5 embryos in whole mount (Fig. 5). The CRABP1 protein has been shown to be present at E9.5 in neural crest cells migrating from r2, r4, and r6 into the developing pharyngeal arches (Maden et al., 1992). Both control (Fig. 5A) and mutant (Fig. 5B) embryos showed extensive labelling of neural crest cells migrating from the hindbrain. In particular, the number and migratory paths of cells emanating from r4, r6, and posterior were not changed in the mutant.

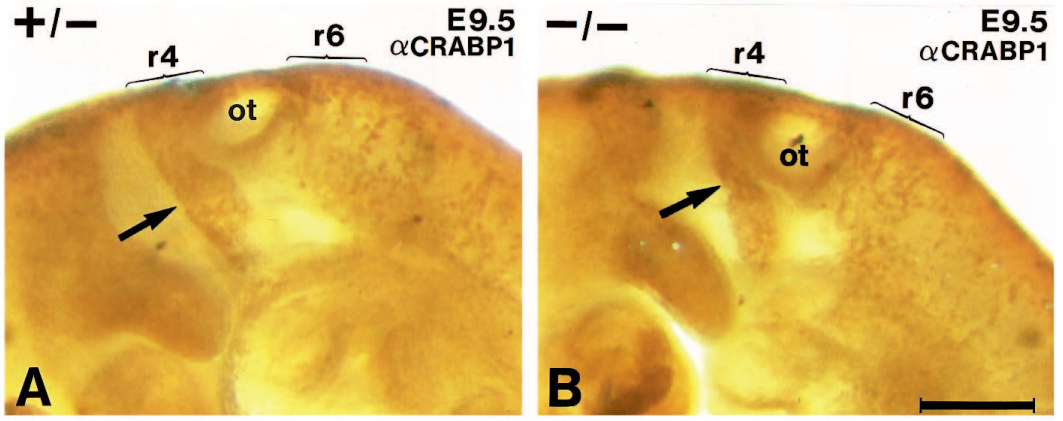

Fig. 5. Visualization of cranial neural crest cells by immunostaining with an anti-CRABP1 antibody. E9.5 embryos were incubated in whole-mount with an antibody against the CRABP1 protein which labels hindbrain neural crest cells. Numerous neural crest cells can be seen migrating from r2, r4, and r6 into the pharyngeal arches in both control (A) and mutant (B) embryos. The arrow indicates the stream of r4-derived neural crest cells. Neural crest cells arising from r6 are seen as individual brown staining cells migrating in a more dispersed pattern. The migratory paths and amounts of neural crest cells at all levels of the hindbrain are the same in both embryos. r, rhombomere; ot, otocyst. Scale bar, 480 μm.

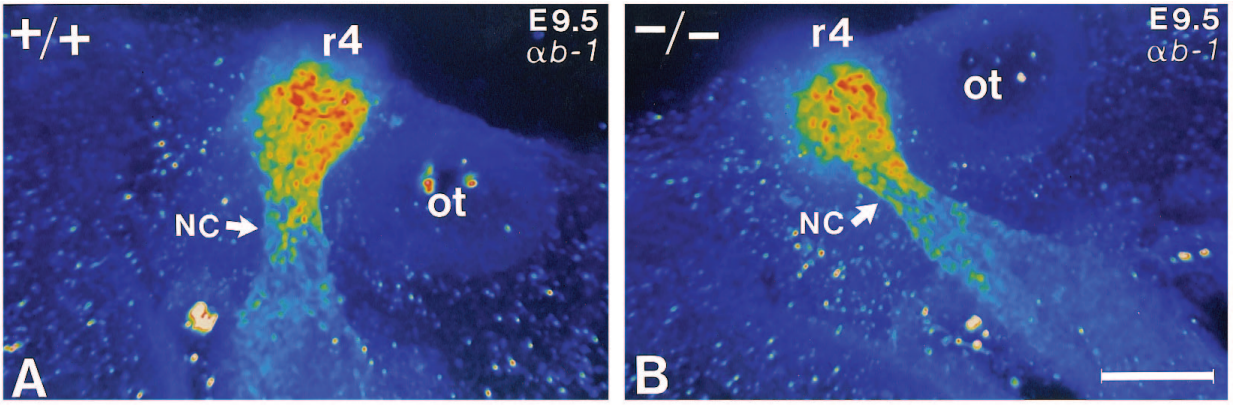

Fig. 6. Visualization of rhombomere 4-derived neural crest in *Hoxa-3* mutant and control embryos by anti-Hoxb-1 antibody. The Hoxb-1 antibody was incubated with E9.5 embryos and localized by immunofluorescence. Embryos were analyzed by confocal microscopy, and optical sections were compiled to generate the image shown. Dorsal is up, cranial is to the left. The Hoxb-1 protein is present in rhombomere 4 and its associated migrating neural crest (arrow). Both the quantity and migratory path of the neural crest appear identical in the control (A) and mutant (B) embryos. r4, rhombomere 4; ot, otocyst; NC, neural crest. Scale bar, 150 μm.

In addition to the CRABP1 gene, the expression patterns of several *Hox* genes were examined in the *Hoxa-3* mutant embryos. The distribution and quantity of *Hoxa-2*-labeled neural crest cells, emanating from r4 and migrating into arch 2, were not grossly altered in *Hoxa-3*⁻ homozygous embryos (Fig. 3). In addition, we prepared an antibody against Hoxb-1 protein and used it in whole-mount immunofluorescence as an independent marker for r-4-derived neural crest. Fig. 6A shows compiled confocal images of an E9.5 immunostained wild-type embryo. At this stage, *Hoxb-1* is expressed in the hindbrain only in r4 and its associated migrating neural crest (Wilkinson et al., 1989; Frohman et al., 1990; Murphy and Hill, 1991). Comparison of the wild-type pattern with that of the mutant (Fig. 6B) revealed no differences.

A more direct way to address whether cells that normally express *Hoxa-3* are deleted or show aberrant migratory paths is to examine the expression of *Hoxa-3* in normal and in mutant embryos. The *Hoxa-3* mutant allele produces a fusion transcript initiated from the *Hoxa-3* promoter that contains *Hoxa-3* RNA sequences 5′ to the insertion of the *neo*ʳ cassette and terminates at the cassette's polyadenylation site. Fig. 7 shows whole-mount in situ hybridization of a control and *Hoxa-3* mutant embryo using sequences 5′ of the *Hoxa-3* homeobox as a probe. The cells that normally express *Hoxa-3*, including the neural crest, are present in the mutant embryo and are not distinguishable in number or distribution from those in the control embryo. These results also suggest that normal *Hoxa-3* protein is not required for the expression of the *Hoxa-3* gene at this stage of development.

Similar analyses performed using probes for the paralogous genes *Hoxb-3* and *Hoxd-3* showed no changes in the expression of either of these genes in *Hoxa-3* mutant embryos relative to wild-type embryos. These genes are expressed in overlapping domains with *Hoxa-3* in the hindbrain, migrating neural crest and neural crest-derived mesenchyme of the 3rd and 4th arches (Hunt et al., 1991a; Sham et al., 1992; Fig. 1A)

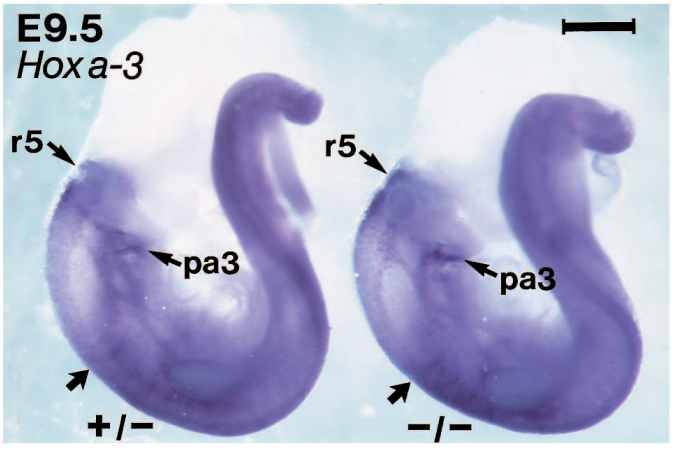

Fig. 7. Comparison of *Hoxa-3* expression in *Hoxa-3* control and mutant embryos. A probe, which encodes the 1st exon and is located 5′ of the *neo*^{r} insertion in the *Hoxa-3* mutation, was used in whole-mount in situ hybridization of +/– and –/– E9.5 embryos. Cranial is up, dorsal is to the left. The pattern of expression is the same in both embryos, including cranial limits in the hindbrain (r5), pharyngeal arches (pa3), and somites (arrows). r, rhombomere; pa, pharyngeal arch. Scale bar, 600 μm.

providing additional evidence that the *Hoxa-3* mutation does not affect neural crest migration (data not shown). These results also show that *Hoxa-3* is not required for the proper expression of either of its paralogues.

Pax-1 expression and the thymus defect in *Hoxa-3* mutants

In the absence of a detectable defect in the production or distribution of neural crest in *Hoxa-3* mutant embryos, the potential exists for a defect in the inductive or differentiative capacity of these cells. This was investigated by examining the embryological origins of the thymus and thyroid defects in *Hoxa-3*$^{-}$ mutant mice. These two organs arise, at least in part, from the 3rd and 4th pharyngeal pouches, respectively (Fig. 1B; Moore and Persaud, 1993). Their development involves interactions between several embryonic cell types (Auerbach, 1960; Rogers, 1971; Bockman and Kirby, 1984).

Thymus development begins with the proliferation of cells in the posterior part of the 3rd pharyngeal pouch at approximately E11.0 (Fig. 1B). The thymic primordia then migrate ventrally to fuse at the midline of the throat (Fig. 1C). Normal thymus development requires the properly timed interactions of pouch endoderm, neural crest-derived arch mesenchyme, and possibly the surface ectoderm from the 3rd pharyngeal cleft (Auerbach, 1960; Cordier and Haumont, 1980; Bockman and Kirby, 1984; Kuratani and Bockman, 1990). *Hoxa-3* is expressed in two of these cell types, the neural crest-derived mesenchyme, and the endodermal cells of the 3rd pharyngeal pouch (Fig. 2, pa3 and pa4, pp3). Genes that are expressed in each of these cell types were used as molecular markers to determine the earliest stage at which a defect in thymus development could be detected. Embryos were initially analyzed at E10.5, after neural crest migration is complete, but before overt thymus development is detectable.

As discussed above, *Hoxa-2*, *Hoxb-3* and *Hoxd-3* are expressed in domains overlapping those of *Hoxa-3* in the 3rd and 4th arch mesenchymal cells, and their expression patterns were not altered in *Hoxa-3* mutants at E10.5 (Fig. 3B,D and data not shown). Another cell type-specific marker in this region is a transcript originating from the antisense strand of the *Hoxb-3* locus. Neither the complete structure of this transcript nor the nature of the gene product encoded by this transcript has been determined. The expression of this transcript, referred to as '*b-3s*,' in the rhombomeres of the E9.5 hindbrain, has been reported previously (Swiatek and Gridley, 1993). At E10.5 in the pharyngeal arch region, *b-3s* is detected in the surface ectoderm covering the arches, as well as in a subset of cells in the 2nd arch mesenchyme. Fig. 8 shows hybridization to the *b-3s* transcript in sections of wild-type and homozygous mutant embryos. No difference in this expression pattern was detected. The number and morphology of these cells also appeared the same. These results indicate that there is no deficiency or defect in the mesenchymal or surface ectoderm cells as detected by these 4 markers prior to overt thymus development.

The endodermal cells of the 3rd pharyngeal pouch were examined using two markers, *fgf-3* and *pax-1*. At E10.5, *fgf-3* is transiently expressed in the posterior half of the pharyngeal pouch endoderm (Wilkinson et al., 1988). Fig. 9 shows whole-mount in situ hybridization of *fgf-3* RNA in the pharyngeal

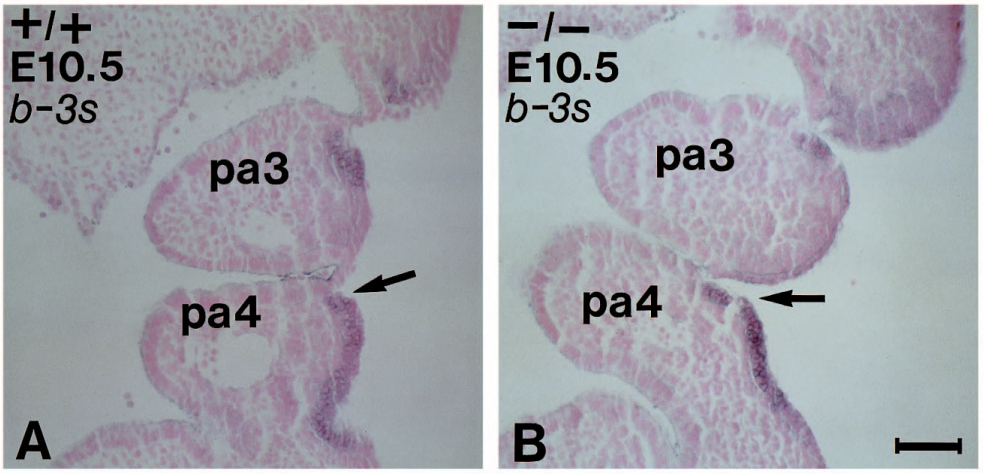

Fig. 8. Expression of the *b-3s* transcript in pharyngeal cleft surface ectoderm. This transcript originates from the antisense strand of the *Hoxb-3* gene, and is detected using a *Hoxb-3* sense strand probe. E10.5 wild-type and *Hoxa-3*$^{-/-}$ embryos were stained in whole mount for the *b-3s* transcript, and then embedded in paraffin and sectioned coronally at 10 μm. Each panel shows the right half of a coronal section. Cranial is up. Expression in both the +/+ (A) and –/– (B) embryos is seen primarily in the surface ectoderm covering the pharyngeal arches and in the pharyngeal clefts. Arrow indicates expression in the third pharyngeal cleft and surface ectoderm covering arch 4. pa, pharyngeal arch. Scale bar, 100 μm.

pouches of *Hoxa-3* control and mutant embryos. No difference was seen in the expression of this marker in the third pouch.

Pax-1 expression in the 3rd pharyngeal pouch begins at E9.5 and continues in this region throughout thymus development (Deutsch et al., 1988; R. Balling, personal communication). At the initiation of *pax-1* expression in the 3rd pouch, differences in *Hoxa-3* control and mutant embryos were not evident (Fig. 10A,B; pp3). However, by E10.5 there is a marked reduction in the level of *pax-1* expression, specifically in the 3rd pouch of *Hoxa-3*⁻ homozygotes (Fig. 10C,D; pp3). By E11, *pax-1* expression is not detectable in the 3rd pouch of the mutant (Fig. 8E,F; pp3). At this stage, the second arch is beginning to overgrow the third arch, partially obscuring the 3rd pouch (Fig. 1B); however, expression in the 3rd pouch of control embryos was readily detected. Expression of *pax-1* at other sites, including the 1st and 2nd pouches and the somites, was not affected by the *Hoxa-3* mutation (Fig. 10 and data not shown).

The differences in the level of *pax-1* expression in the 3rd pouch as seen by whole-mount in situ hybridization could be due to a reduction in cell number rather than to a reduction in expression at the level of individual cells. The fact that the expression levels of other molecular markers labeling these cells were not reduced argues against this possibility. Further, in sections through the pouch region, individual 3rd pouch cells showed reduced levels of *pax-1* expression relative to control sections (Fig. 11) whereas *pax-1* expression in the cells of the 2nd pouch of control and mutant embryos was equivalent. The results showing that the expression of *fgf-3, Hoxa-2* and *Hoxa-3* were unaffected in the same cells that show reduced *pax-1* expression in mutant embryos are consistent with a requirement for *Hoxa-3* in the maintenance of *pax-1* expression in the 3rd pharyngeal pouch. As animals mutant for *pax-1* show thymus hypoplasia (Dietrich and Gruss, 1995; Rudi Balling, personal communication), these results suggest that *pax-1* is downstream of *Hoxa-3* in a regulatory pathway required for thymus development.

The *Hoxa-3* mutation affects the formation of both the follicular and parafollicular cells of the thyroid

The thyroid gland is formed by the fusion of two structures of separate embryological origin, the thyroid diverticulum and the ultimobranchial body (see Fig. 1B,C; Hilfer, 1968; Rogers, 1927, 1971). The diverticulum is formed from the endodermal epithelium in the floor of the pharynx beginning at E10.5. These cells give rise to the thyroxin-producing follicular cells in the mature thyroid. The ultimobranchial body is formed from the 4th pouch and is composed primarily of neural crest-derived cells (Pearse and Polak, 1971; LeLievre and LeDouarin, 1975; Fontaine, 1979). These cells give rise to the parafollicular or C-cells, which produce calcitonin (Pearse and Carvalheira, 1967; Moseley et al., 1968; Williams et al., 1989). The ultimobranchial body and the thyroid diverticulum migrate from their respective sites of origin to their final position in the throat and then fuse, such that the two cell types are completely intermixed in the mature thyroid (Fig. 1C). *Hoxa-3* is expressed in the floor of the pharynx, the developing thyroid diverticulum, and in the neural crest mesenchyme of the 4th pharyngeal arch, which will give rise to the ultimobranchial body (Gaunt, 1988; Hunt et al., 1991a). *Hoxa-3* is also expressed in the 4th pharyngeal pouch endoderm (Fig. 2B).

An antibody against calcitonin was used to identify C-cells in transverse sections of *Hoxa-3* control and mutant newborn animals. The calcitonin-producing cells appear brown against a nuclear counterstain. In control animals, the thyroid is a bilobed structure, with two large lateral lobes joined across the ventral midline at their posterior aspects by the isthmus. Fig. 12A shows a transverse section through one lateral lobe of a control animal. Both calcitonin-producing parafollicular cells (brown stain) and diverticulum-derived follicular cells (f) were present. Calcitonin-producing cells were numerous and could be found throughout the lobe, but were concentrated in the more anterior and dorsal portions of the lateral lobes. Calcitonin-positive cells were not present in the isthmus (not shown). Although absolute numbers of calcitonin-positive cells varied between control animals, their placement within the thyroid and the overall size and morphology of the thyroid itself was consistent.

In *Hoxa-3* mutants, defects were present in both the calci-

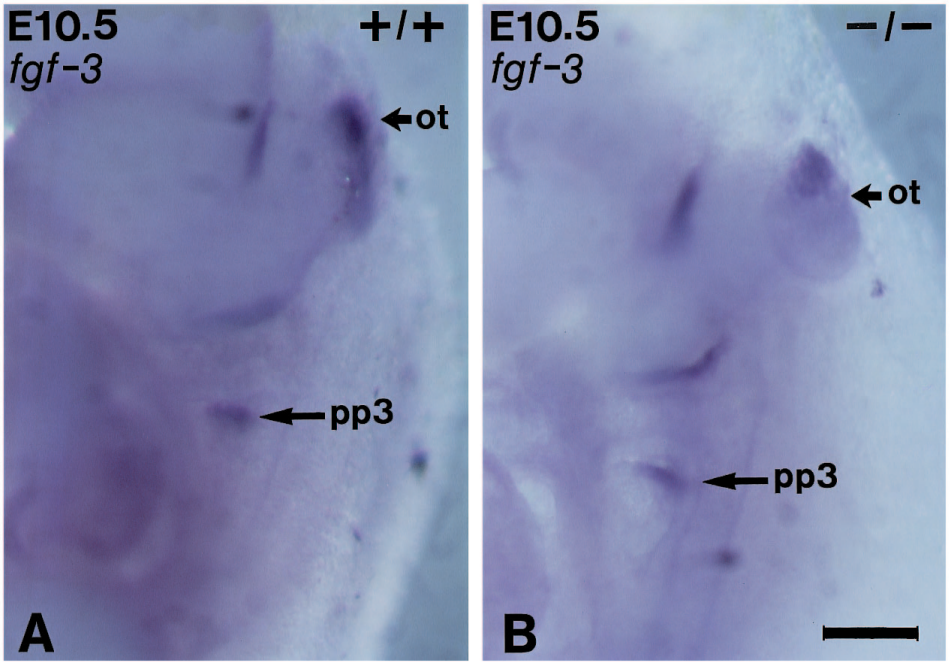

Fig. 9. Expression of the *fgf-3* gene in the pharyngeal pouches of *Hoxa-3*$^{+/+}$ and *Hoxa-3*$^{-/-}$ embryos. (A) Ventrolateral view of the pharyngeal pouches of an E10.5 wild-type embryo stained by whole-mount in situ hybridization for *fgf-3* expression. Cranial is up. Expression in the third pharyngeal pouch is indicated (pp3). Expression in the otocyst is also visible (ot). (B) Similar view of a *Hoxa-3*$^{-/-}$ embryo. Note the identical expression in the third pouch (pp3). The apparent difference in otocyst staining is due to a slight difference in the photographic angle. pp, pharyngeal pouch; ot, otocyst. Scale bar, 175 μm.

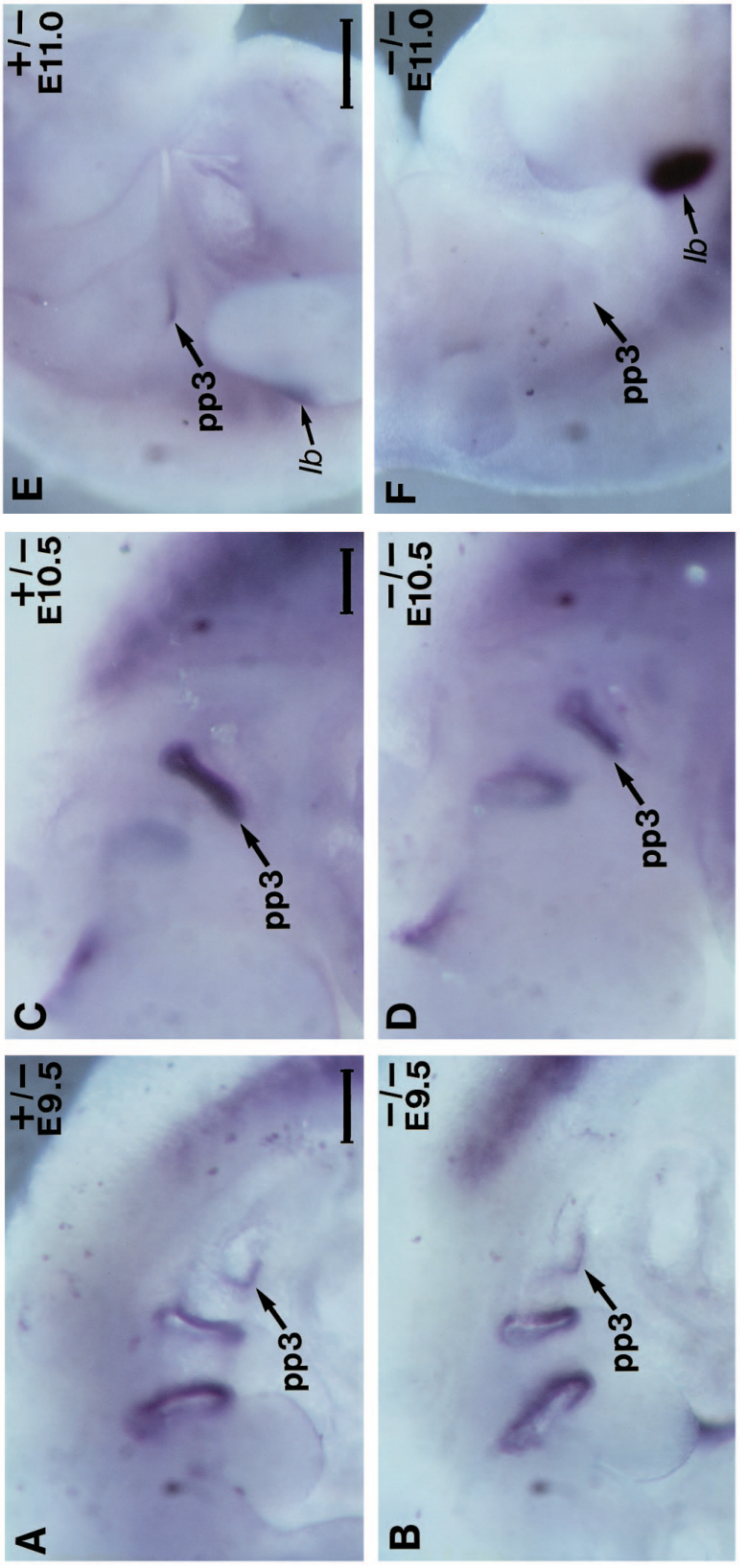

Fig. 10. Time course of *pax-1* gene expression in the pharyngeal region of *Hoxa-3* mutant and control embryos. *Pax-1* expression was followed using whole-mount in situ analysis from E9.5 to E11. The third pharyngeal pouch is indicated in each panel (pp3). (A,B) At E9.5, expression is just beginning in the third pouch of both control (A) and mutant (B) embryos. (C) By E10.5, expression in the third pouch of the control embryo is very strong. (D) In the mutant at E10.5, expression in the third pouch is markedly reduced, while other sites of expression are unaffected. (E) Expression of *pax-1* in the 3rd pharyngeal pouch at E11.0. (F) In the mutant embryo, *pax-1* expression is not detectable in the third pouch. *Pax-1* expression in the forelimb bud (lb) is much more visible in the mutant because of a difference in the angle of the limb. In A-D cranial is to the left, dorsal is up. In E-F cranial is up, dorsal is to the left. pp3, third pharyngeal pouch; lb, limb bud. Scale bars, (A,B) 175 μm; (C,D) 200 μm; (E,F) 400 μm

tonin-positive C-cell population and in the follicular cells which form the body of the thyroid. Results from the analysis of five mutant animals are summarized in Table 1. Mutant animals were hypoplastic for calcitonin-producing cells, with four of the five animals showing a reduction of 50% or more in the number of calcitonin positive cells in the thyroid itself. This reduction was frequently unilateral, with one side of the animal showing a relatively normal thyroid lobe while the other side either contained no calcitonin-positive cells or completely lacked a thyroid lobe. Three animals also displayed a dorsal and cranially placed vesicular structure in which virtually every cell is calcitonin-positive (Fig. 12B-D; ub). These vesicles were either associated with thyroid lobes lacking calcitonin-positive cells (B and C) or were present where the lobe was completely deleted (D, star). This structure varied in size and had no visible connection to the thyroid. These calcitonin-positive vesicles may represent persistent ultimobranchial bodies that failed to fuse with the thyroid diverticulum.

The structure of the thyroid lobe itself was also affected in *Hoxa-3*⁻ homozygotes and varied considerably even on opposite sides of the same mutant animal. The overall size and shape of the thyroid lobes were variable, and the isthmus was either displaced cranially or was completely absent in all mutants examined. As mentioned above, the thyroxin-producing follicular cells were either normal in number or were totally absent on one side. Follicles were formed, but generally appeared to be larger than those formed in control animals (compare Fig. 12A with B and C; f) and could be completely disorganized, lacking the characteristic rosette of secretory cells seen in normal sections (Fig. 12B; f, white arrow). The severity of defects in the follicular lobes of the thyroids correlated with the presence of a persistent ultimobranchial body. In all cases, the existence of a persistent body was associated with the lack of an isthmus and the deletion or reduction by approximately 50% of the thyroid lobe on the same side.

Defect in the epithelial lining of the trachea

Although many of the defects observed in *Hoxa-3*⁻ mutant mice are found in tissues derived from or patterned by mesenchymal neural crest, there are exceptions. For example, the epithelial lining of the trachea, similar to the thyroid diverticulum, is derived from the ventral endodermal epithelium of the embryonic pharynx. However, the tracheal epithelium is not known to have any interactions with the neural crest. *Hoxa-3* is expressed in the floor of the pharynx at E12.5 (Gaunt, 1988). Examination of the tracheal lining in newborn control animals showed the typical columnar basal epithelial morphology (Fig. 13A). In all mutant animals examined, this layer of cells was poorly organized, with cells piling up on each other (Fig. 13B). The cells composing this layer had lost the appearance of basal epithelial cells, varying in size, shape and polarity.

Table 1. Thyroid phenotypes in newborn *Hoxa-3* mutant mice

	mutant no.									
	1		2		3		4		5	
	L	R	L	R	L	R	L	R	L	R
Thyroid tissue	++†	+	–	++	++	+	++	–	++	++
Calcitonin in thyroid	+‡	–	–	++	++	–	++	–	++	++
Ectopic UB*	–	Yes	Yes	–	–	Yes	–	ND	–	–
Isthmus	Absent		Absent		Absent		Present§		Present§	

*Ectopic ultimobranchial bodies, all positive for calcitonin.
†Thyroid lobe was normal in size but abnormally shaped.
‡Number of calcitonin positive cells was reduced approximately 20×; intensity of staining was also reduced relative to controls.
§Isthmus is abnormally positioned.
L = left side, R = right side, ++ = normal, + = reduced relative to normal, – = none.

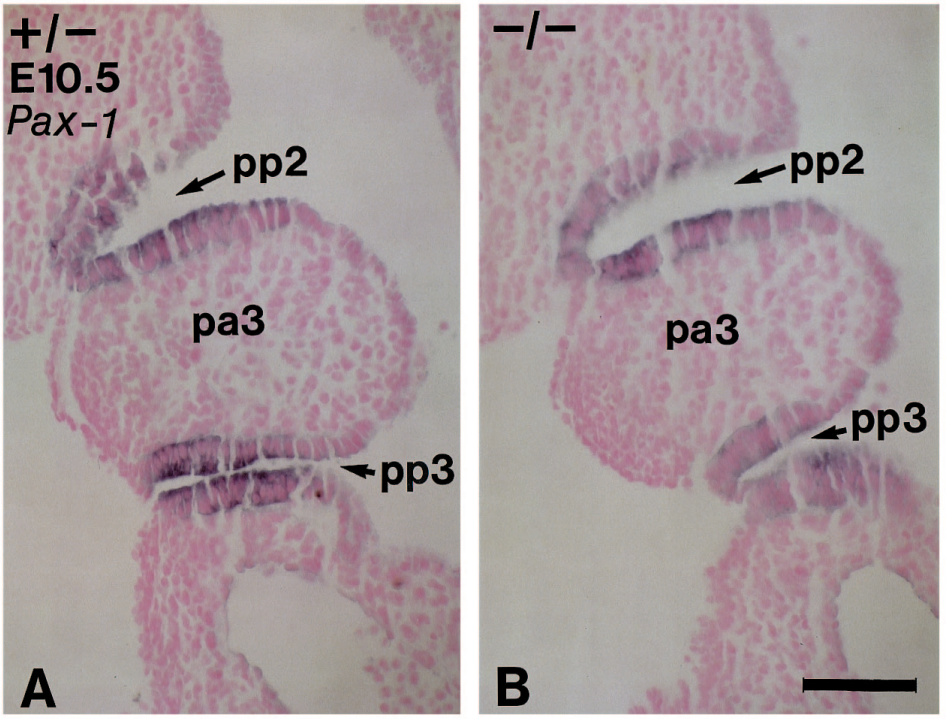

Fig. 11. Loss of *pax-1* gene expression in the third pharyngeal pouch at the cellular level. E10.5 control and mutant embryos stained in whole mount for *pax-1* RNA expression were embedded in paraffin and sectioned coronally at 10 μm. Each panel shows the left half of a coronal section. Cranial is up. (A) Strong expression is seen in the endodermal epithelial cells in both the second (pp2) and third (pp3) pouches of the control embryo. (B) Expression in the *Hoxa-3*$^{-/-}$ embryo in the second pouch is comparable to the control (pp2). The cells of the third pouch, however, show markedly reduced expression relative to the control (pp3). pa, pharyngeal arch; pp, pharyngeal pouch. Scale bar, 75 μm.

DISCUSSION

Loss of *Hoxa-3* does not appear to affect the expression of other *Hox* genes

Defects observed in mice with a single disrupted *Hox* gene may be due in part to effects on the expression of other *Hox* genes. Such an effect could result from disruption of a regulatory relationship among *Hox* genes or by an inactivation of *cis* regulatory elements due to the introduction of a selectable marker into the locus. In the case of *Hoxa-3*, neither the expression of the neighboring gene *Hoxa-2* nor the expression of the two paralogous genes *Hoxb-3* and *Hoxd-3* were affected by the *Hoxa-3* mutation. Therefore, effects on the regulation of other *Hox* genes we examined do not account for the phenotypes seen cranial to the reported expression domain of *Hoxa-3*. Alternative hypotheses to explain these anterior defects include: (1) that the affected structures are formed from a mixture of cells that originate both within and outside the *Hoxa-3* expression domain and that the defects in the anterior structures reflect the contribution of the defective cells that arise in the *Hoxa-3* domains; (2) that the early expression domain of *Hoxa-3* may include cells not apparent in the later expression patterns which contribute to more cranial structures; or (3) indirect effects of the *Hoxa-3* mutation on the formation of structures anterior to the *Hoxa-3* expression domain arising, for example, from *Hoxa-3* mutant defects in vascularization. We have examined *Hoxa-3* expression in E8.5 embryos and a rostral shift in expression relative to the boundaries in E9.5 and E10.5 embryos is not apparent. However, due to the smaller size of the embryo and the paucity of morphological markers at this time, it is difficult to define precisely the position of the cranial boundary of *Hoxa-3* expression in the hindbrain before rhombomere boundaries are established.

Hoxa-3 appears to have primary functions in both endoderm and neural crest

The *Hoxa-3* mutant phenotype has striking similarities to those caused

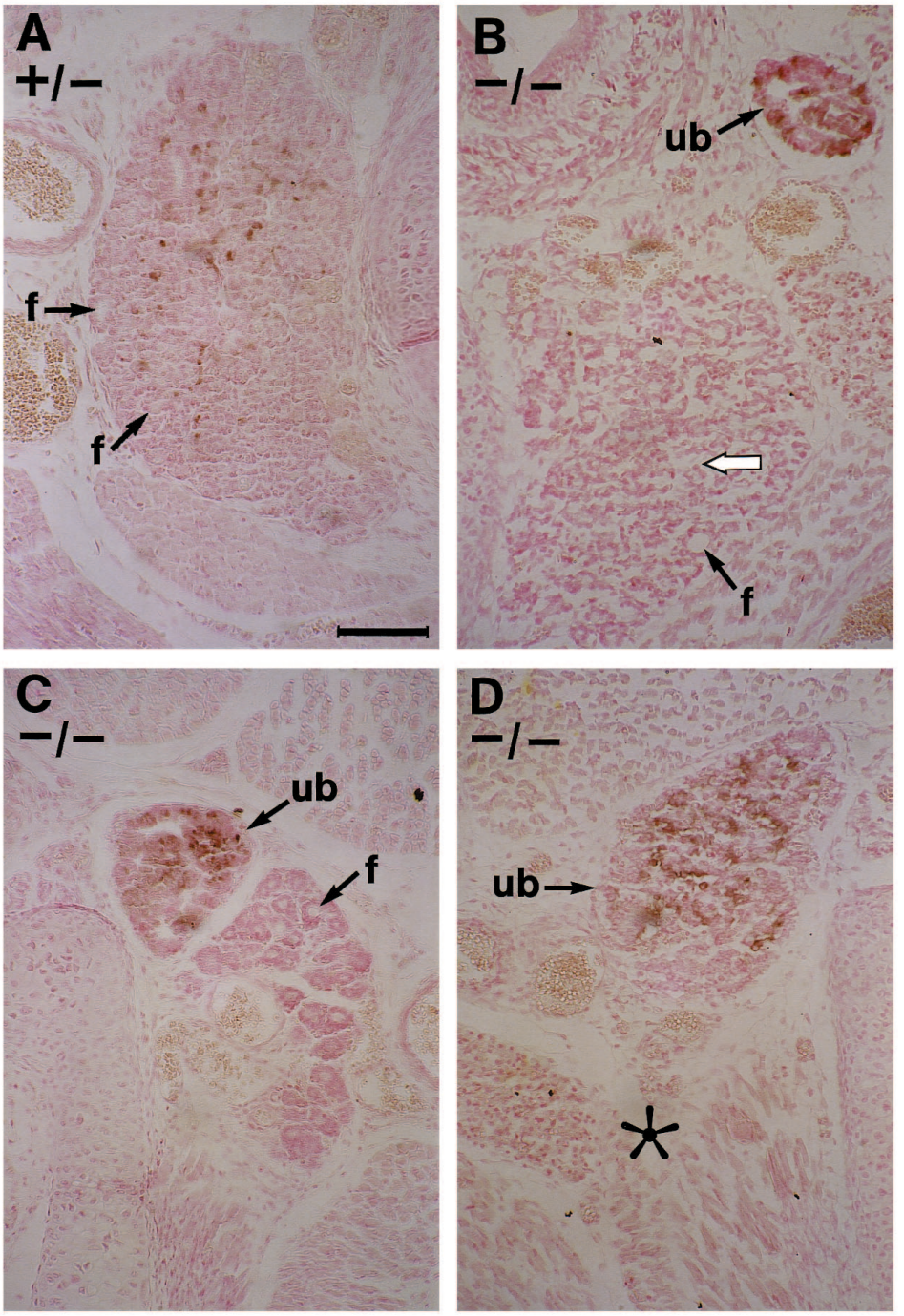

Fig. 12. The presence of persistent ultimobranchial bodies in the *Hoxa-3* mutant thyroid phenotype. 10 μm transverse sections of newborn animals were stained with an anti-calcitonin antibody, which shows calcitonin-positive cells as brown. Panels show either the left or right side of a control (A) or three different mutants (B-D). Dorsal is up. (A) Left side of a wild-type thyroid, with numerous calcitonin-positive cells throughout the lobe, particularly in the dorsal half. Rosette-shaped follicles are also present (f). (B) Right side of a *Hoxa-3* mutant thyroid. The cells in the main body of the thyroid are disorganized (white arrow), with only a few large follicles formed (f). Note the dorsally placed vesicle which is strongly positive for calcitonin (ub). (C) Right side of another *Hoxa-3* mutant. The thyroid is composed entirely of very large follicles (f). A vesicle positive for calcitonin is also present dorsal to the thyroid lobe (ub). (D) Left side of a third *Hoxa-3* mutant. In this case, no thyroid tissue is present on this side of the animal (star). A large calcitonin-positive body, which appears to be entirely composed of parafollicular C-cells, is present slightly dorsal to the normal position of the thyroid (ub). f, follicle; ub, ultimobranchial body. Scale bar, 100 μm.

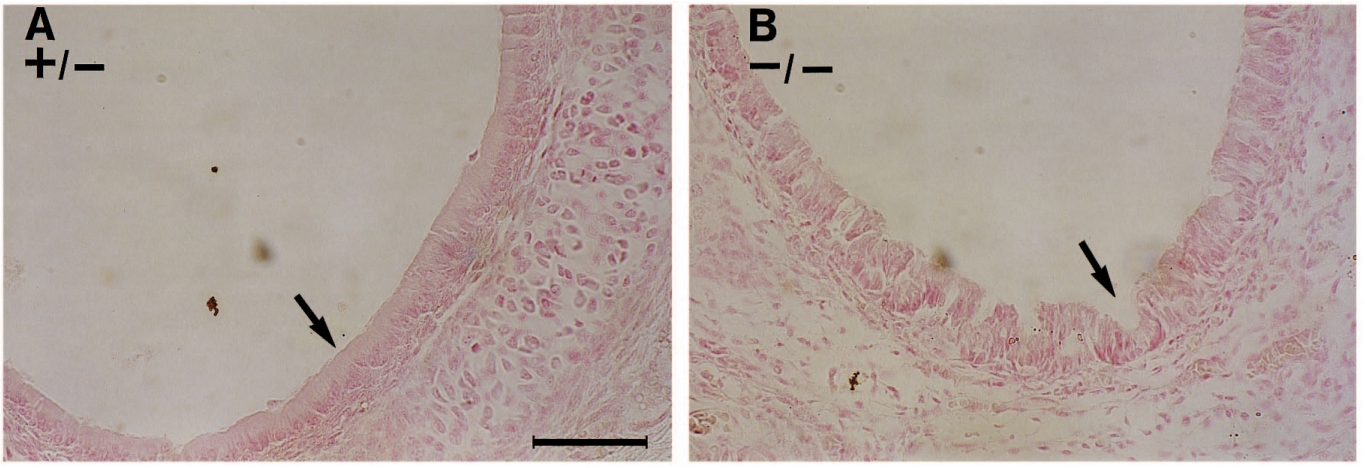

Fig. 13. The epithelial lining of the trachea is abnormal in *Hoxa-3* mutant animals. Transverse sections of control and *Hoxa-3* mutant newborns stained with Nuclear Fast Red. Dorsal is up. Nuclei are stained dark pink. (A) In a heterozygous control, the tracheal lining has a basal columnar epithelial structure (arrow). (B) In a *Hoxa-3* mutant, the epithelial layer is disorganized, with cells piling on top of each other, sometimes forming a convoluted surface (arrow). Cells do not have a uniform columnar appearance. Scale bar, 75 μm.

by neural crest ablation in the chick, particularly in tissues derived from the 3rd and 4th pharyngeal arches and pouches (Bockman and Kirby, 1984; Bockman et al., 1989; Kuratani and Bockman, 1990). All of the mesenchymally derived and patterned structures arising from these arches are affected similarly by ablation and by the loss of *Hoxa-3*. The dye injection and marker gene analysis show, however, that there is no major change in the amount or distribution of neural crest cells in *Hoxa-3*⁻ mutant embryos. Further, neural crest ablation leads to a marked reduction in the amount of mesenchyme present in the pharyngeal arches, a phenotype not seen in the *Hoxa-3* mutants (Bockman et al., 1989; Figs 8 and 11). None of the methods used to follow neural crest, including dye injection or marker gene analysis, would detect the loss of small subpopulations of neural crest in *Hoxa-3*⁻ homozygotes. However, it should be kept in mind that the *Hoxa-3* mutation affects multiple tissues derived from or patterned by mesenchymal neural crest and that extensive premigratory neural crest ablation phenocopies the *Hoxa-3* mutation. Thus it is unlikely that the loss of a small subpopulation of neural crest cells in *Hoxa-3*⁻/*Hoxa-3*⁻ mice could account for the complex phenotype observed in these mice.

Because changes in overall neural crest production or migration are not observed, the defects seen in *Hoxa-3*⁻ mutant mice may result from an intrinsic defect in neural crest differentiation and/or in its capacity to pattern the surrounding tissues. As *Hoxa-3* is expressed in both the neural crest-derived mesenchyme and in the pharyngeal pouch endoderm of the 3rd and 4th arch region, the defects in the thymus and thyroid could be the result of defects in either or both of these tissues. In the case of the thymus defect, the expression pattern of *pax-1* in the *Hoxa-3* mutant embryos suggests that *pax-1* is specifically down regulated in the 3rd pharyngeal pouch endoderm before overt thymus development begins. The expression of *pax-1* is initiated normally, but is reduced during pouch development, suggesting that *Hoxa-3* may be required for maintenance (but not initiation) of *pax-1* expression in these cells. No changes in the expression patterns of any other marker we tested for surface ectoderm, mesenchyme or endoderm were found. This essentially normal pattern of gene expression argues that the cells in this region are present and overtly normal. These results indicate that the specific loss of *pax-1* expression results from a direct or indirect regulatory interaction with *Hoxa-3*, implying that *pax-1* functions downstream of *Hoxa-3* in these cells.

The comparison between the expression of *fgf-3* and *pax-1* in *Hoxa-3* control and mutant embryos is particularly instructive since mouse mutants for each of these genes are available. The *fgf-3* mutant mice show defects in tail and inner ear development but not in thymus development (Mansour et al., 1993). However, mice that carry deletions at the *pax-1* locus, $undulated^{extensive}$ and $Undulated^{shorttail}$, have defective thymus development (Dietrich and Gruss, 1995; Wallin et al., 1994 and Rudi Balling, personal communication). The thymus in these *pax-1* mutant animals is 30-50% smaller than normal, and the number and composition of thymocytes are also abnormal (Rudi Balling, personal communication). The observation that *pax-1* mutants have thymus defects that are similar to but weaker than the *Hoxa-3* defects again argues that *pax-1* is downstream of *Hoxa-3*. However, down regulation of *pax-1* cannot be entirely responsible for the thymus defect observed in *Hoxa-3*⁻ mutant mice. One possibility is that *Hoxa-3*⁻/*Hoxa-3*⁻ mice have a defect in both pouch endoderm and pharyngeal arch neural crest-derived mesenchyme and that together these two defects cause the severe thymus phenotype.

The thyroid hypoplasia observed in *Hoxa-3*⁻ mutant mice may also have its origins in multiple tissues. These mutant mice show defects in both the follicular cells, which are of endodermal origin, and in the parafollicular cells (C-cells) which are derived from mesenchymal neural crest cells. The number of follicular and parafollicular cells is severely reduced in *Hoxa-3*⁻ homozygotes. However, C-cells are often observed in a vesicle which may represent a defective ultimobranchial body. In all cases, the number of thyroid follicular cells is reduced and the organization of these cells in the thyroid lobe is defective. Little is known about how the thyroid diverticulum and the ultimobranchial body recognize each other, fuse and subsequently form the mature thyroid gland. It is also not known whether inductive interactions between these two tissues are important in forming the mature thyroid gland. On

the one hand, cells capable of making terminal differentiation markers (e.g. calcitonin for C-cells and thyroxin for follicular cells) are present in *Hoxa-3*$^{-}$ mutant mice. On the other hand, the organization and number of these cells within the thyroid lobes is aberrant. It is also possible that a defect in the endoderm of the 4th pharyngeal pouch could contribute to the production of a defective ultimobranchial body. These results are consistent with a role for *Hoxa-3* in both cell types, and support the possibility that interactions between these cells are important in the development of the mature gland.

The variable expressivity of the thyroid phenotype, particularly between the different sides of the same mutant animal, suggests that another gene or genes is partially compensating for the *Hoxa-3* mutation during thyroid development. An attractive candidate for this compensatory gene is *Hoxb-3*, a paralogue of *Hoxa-3*. Previously, we have shown that paralogous *Hox* genes can interact in the formation of a structure in which they are both expressed (Condie and Capecchi, 1994). *Hoxb-3* is expressed in the thyroid diverticulum and in the mesenchyme surrounding the 4th pharyngeal arch, but not in the 4th pharyngeal pouch endoderm. Interestingly, using a transient transfection assay in cultured mammalian cells, it has been suggested that *Hoxb-3* may regulate the expression of *thyroid transcription factor-1, ttf-1* (Guazzi et al., 1994). This gene is an early differentiation marker for thyroid cells and is thought to be involved in the activation of thyroid specific genes such as *thyroglobulin* and *thyroperoxidase* (Civitareale et al., 1989; Francis-Lang et al., 1990; Guazzi et al., 1990; Lazzaro et al., 1991). The transfection results implicate *Hoxb-3* in thyroid development. The analysis of mice mutant for *Hoxb-3*, as well as mice mutant for both *Hoxa-3* and *Hoxb-3*, will directly address the possibility of functional redundancy between these two genes in thyroid development. A contributing factor in the thyroid phenotype variability could also be that another cell type is able to partially compensate for defective cells in the *Hoxa-3* mutants.

Analysis of the thymus and thyroid defects provides evidence that *Hoxa-3* functions at different times during development. The thymus defect is apparent early in thymus development and results in the total or near total deletion of the thymus. In contrast, both components of the thyroid gland form and migrate to their final location, but fail to complete normal development. In this case, terminally differentiated cell types are formed, even in the apparent absence of fusion between the ultimobranchial body and the thyroid diverticulum. Both the thymus and thyroid defects are consistent with a defect in the patterning or differentiation of the mesenchymal neural crest. The results also suggest that a *Hoxa-3* dependent differentiation of endodermal cells is an important component of these developmental pathways. Finding defects in endoderm-derived tissue of the tracheal lining, which has no apparent connection to mesenchymal neural crest, suggests that the endodermal defects in the thymus and thyroid could also be intrinsic, rather than the result of interactions with mesenchymal neural crest.

Hoxa-3 and DiGeorge syndrome

DiGeorge syndrome is characterized as a haploinsufficiency marked by hypoparathyroidism, thymic and thyroid hypoplasia, cardiac deficiencies, and craniofacial abnormalities. This set of defects is remarkably similar to those observed in *Hoxa-3*$^{-}$/*Hoxa-3*$^{-}$ mice. Two studies have been published analyzing the presence of calcitonin-producing cells in the thyroid tissue of DiGeorge patients (Burke et al., 1987; Pueblitz et al., 1993). Both studies found reduced numbers of C-cells in DiGeorge patients, relative to controls, as well as a subset with no calcitonin-positive cells. The amount of thyroid tissue was also variably reduced in DiGeorge patients. Comparison of the results from these studies with the *Hoxa-3* phenotype are striking. Both studies found that thymic hypoplasia and hypoparathyroidism were more severe and more penetrant phenotypes than the thyroid defects, which is also the case for the *Hoxa-3* mutants. The thyroid defects of DiGeorge patients ranged from normal thyroid appearance and presence of calcitonin positive cells to hypoplastic thyroid with a complete absence of calcitonin-containing cells. The same range of defects was seen in the thyroid lobes of *Hoxa-3* mutants. The similarities are particularly striking considering that the patient materials available for the DiGeorge cases were frequently incomplete, which could also account for the fact that neither study identified persistent ultimobranchial bodies such as those seen in the present study. These similarities in the details of the DiGeorge and *Hoxa-3* phenotypes further underscore the utility of the *Hoxa-3* mouse as a model for DiGeorge syndrome.

We thank R. Balling and P. Gruss for providing information on *pax-1* and the *undulated* thymus phenotypes prior to publication, and R. Balling for providing the *pax-1* RNA probes. We thank C. V. E. Wright for providing protocols and advice for the antibody work. We also thank L. Oswald for help with the preparation of the manuscript, and N. R. M. thanks B. Condie for helpful discussions. N. R. M. was supported by NRSA fellowship no. 1 F32 NS09332-01.

REFERENCES

Auerbach, R. (1960). Morphogenetic interactions in the development of the mouse thymus gland. *Dev. Biol.* **2**, 271-284.

Bockman, D. E. and Kirby, M. L. (1984). Dependence of thymus development on derivatives of the neural crest. *Science* **223**, 498-500.

Bockman, D. E., Redmond, M. E. and Kirby, M. L. (1989). Alteration of early vascular development after ablation of cranial neural crest. *Anat. Rec.* **225**, 209-217.

Burke, B. A., Johnson, D., Gilbert, E. F., Drut, R. M., Ludwig, J. and Wick, M. R. (1987). Thyrocalcitonin-containing cells in the DiGeorge anomaly. *Hum. Pathol.* **18**, 355-360.

Carpenter, E. M., Goddard, J. M., Chisaka, O., Manley, N. R. and Capecchi, M. R. (1993). Loss of *Hox-A1* (*Hox-1.6*) function results in the reorganization of the murine hindbrain. *Development* **118**, 1063-1075.

Chisaka, O. and Capecchi, M. R. (1991). Regionally restricted developmental defects resulting from targeted disruption of the mouse homeobox gene *Hox-1.5*. *Nature* **350**, 473-479.

Chisaka, O., Musci, T. S. and Capecchi, M. R. (1992). Developmental defects of the ear, cranial nerves and hindbrain resulting from targeted disruption of the mouse homeobox gene *Hox-1.6*. *Nature* **355**, 516-520.

Civitareale, D., Lonigro, R., Sinclair, A. J. and DiLauro, R. (1989). A thyroid specific nuclear protein essential for tissue specific expression of the thyroglobulin promoter. *EMBO J.* **8**, 2537-2542.

Condie, B. G. and Capecchi, M. R. (1994). Mice with targeted disruptions in the paralogous genes *Hoxa-3* and *Hoxd-3* reveal synergistic interactions. *Nature* **370**, 304-307.

Cordier, A. C. and Haumont, S. M. (1980). Development of thymus, parathyroids, and ultimobranchial bodies in NMRI and Nude mice. *Am. J. Anat.* **157**, 227-263.

Deutsch, U., Dressler, G. R. and Gruss, P. (1988). *Pax-1*, a member of a paired box homologous murine gene family, is expressed in segmented structures during development. *Cell* **53**, 617-625.

Dietrich, S. and Gruss, P. (1995). Pleiotropic *undulated* phenotypes suggest a role of *Pax-1* for growth processes in mesoderm, endoderm, and neural crest derived structures. *Dev. Biol.* **167 (2)**, 529-548.

Dollé, P., Lufkin, T., Krumlauf, R., Mark, M., Duboule, D. and Chambon,

P. (1993). Local alterations of *Krox-20* and *Hox* gene expression in the hindbrain suggest lack of rhombomeres 4 and 5 in homozygote null *Hoxa-1 (Hox-1.6*) mutant embryos. *Proc. Natl. Acad. Sci. USA* **90**, 7666-7670.

Eriksson, U., Hansson, E., Nordlinder, H., Busch, C., Sundelin, J. and Peterson, P. A. (1987). Quantitation and tissue localization of the cellular retinoic acid-binding protein. *J. Cell. Physiol.* **133**, 482-490.

Fontaine, J. (1979). Multistep migration of calcitonin cell precursors during ontogeny of the mouse pharynx. *Gen. Comp. Endocrinol.* **37**, 81-92.

Francis-Lang, H., Price, M., Martin, U. and DiLauro, R. (1990). The thyroid specific nuclear factor, TTF-1, binds to the rat thyroperoxidase promoter. In *Thyroperoxidase and Thyroid Autoimmunity* (ed. P. Carayon) **207**, pp. 25-32. John Libbey Eurotext Ltd.

Frohman, M. A., Boyle, M. and Martin, G. R. (1990). Isolation of the mouse *Hox-2.9* gene; analysis of embryonic expression suggests that positional information along the anterior-posterior axis is specified by mesoderm. *Development* **110**, 589-607.

Gamer, L. W. and Wright, C. V. E. (1993). Murine *Cdx-4* bears striking similarities to the *Drosophila caudal* gene in its homeodomain sequence and early expression pattern. *Mech. Dev.* **43**, 71-81.

Gaunt, S. J. (1988). Mouse homeobox gene transcripts occupy different but overlapping domains in embryonic germ layers and organs: a comparison of *Hox-3.1* and *Hox-1.5*. *Development* **103**, 135-144.

Gendron-Maguire, M., Mallo, M., Zhang, M. and Gridley, T. (1993). *Hoxa-2* mutant mice exhibit homeotic transformation of skeletal elements derived from cranial neural crest. *Cell* **75**, 1317-1331.

Guazzi, S., Lonigro, R., Pintonello, L., Boncinelli, E., DiLauro, R. and Mavilio, F. (1994). The thyroid transcription factor-1 gene is a candidate target for regulation by Hox proteins. *EMBO J.* **13**, 3339-3347.

Guazzi, S., Price, M., DeFelice, M., Damante, G., Mattei, M.-G. and DiLauro, R. (1990). Thyroid nuclear factor 1 (TTF-1) contains a homeodomain and displays a novel DNA binding specificity. *EMBO J.* **9**, 3631-3639.

Hall, B. K. (1981). The induction of neural crest-derived cartilage and bone by embryonic epithelia: an analysis of the mode of action of an epithelial-mesenchymal interaction. *J. Embryol. exp. Morphol.* **64**, 305-320.

Hall, B. K. (1987). Tissue interactions in the development and evolution of the vertebrate head. In *Developmental and Evolutionary Aspects of the Neural Crest* (ed. P. F. A. Maderson), pp. 215-259. New York: John Wiley.

Hilfer, S. R. (1968). Cellular interactions in the genesis and maintenance of thyroid characteristics. In *Epithelial-Mesenchymal Interactions* (ed. R. Fleischmajer and R. E. Billingham), pp. 177-199. Baltimore: Williams and Wilkins Co.

Hunt, P., Gulisano, M., Cook, M., Sham, M.-H., Faiella, A., Wilkinson, D., Boncinelli, E. and Krumlauf, R. (1991a). A distinct *Hox* code for the branchial region of the vertebrate head. *Nature* **353**, 861-864.

Hunt, P., Wilkinson, D. and Krumlauf, R. (1991b). Patterning the vertebrate head: murine *Hox 2* genes mark distinct subpopulations of premigratory and migrating cranial neural crest. *Development* **112**, 43-50.

Kissinger, C. R., Liu, B., Martin-Blanco, E., Kornberg, T. B. and Pabo, C. O. (1990). Crystal structure of an engrailed homeodomain-DNA complex at 2.8 Å resolution: a framework for understanding homeodomain-DNA interactions. *Cell* **63**, 579-590.

Kuratani, S. and Bockman, D. E. (1990). Impaired development of the thymic primordium after neural crest ablation. *Anat. Rec.* **228**, 185-190.

Lazzaro, D., Price, M., DeFelice, M. and DiLauro, R. (1991). The transcription factor *TTF-1* is expressed at the onset of thyroid and lung morphogenesis and in restricted regions of the foetal brain. *Development* **113**, 1093-1104.

LeLievre, C. S. and LeDouarin, N. M. (1975). Mesenchymal derivatives of the neural crest: analysis of chimaeric quail and chick embryos. *J. Embryol. exp. Morph.* **34**, 125-154.

Lufkin, T., Dierich, A., LeMeur, M., Mark, M. and Chambon, P. (1991). Disruption of the *Hox-1.6* homeobox gene results in defects in a region corresponding to its rostral domain of expression. *Cell* **66**, 1105-1119.

Maden, M., Horton, C., Graham, A. Leonard, L., Pizzey, J., Siegenthaler, G., Lumsden, A. and Eriksson, U. (1992). Domains of cellular retinoic acid-binding protein I (CRABP I) expression in the hindbrain and neural crest of the mouse embryo. *Mech. Dev.* **37**, 13-23.

Mansour, S. L., Goddard, J. M. and Capecchi, M. R. (1993). Mice homozygous for a targeted disruption of the proto-oncogene *int-2* have developmental defects in the tail and inner ear. *Development* **117**, 13-28.

Mark, M., Lufkin, T., Vonesch, J. L., Ruberte, E., Olivo, J.-C., Dollé, P., Gorry, P., Lumsden, A. and Chambon, P. (1993). Two rhombomeres are altered in *Hoxa-1* mutant mice. *Development* **119**, 319-338.

Moore, K. L. and Persaud, T. V. N. (1993). The branchial or pharyngeal apparatus. In *The Developing Human: Clinically Oriented Embryology*, pp. 186-225. Philadelphia: W. B. Saunders Company.

Moseley, J. M., Mathews, E. W., Breed, R. H., Galante, L., Tse, A. and MacIntyre, I. (1968). The ultimobranchial origin of calcitonin. *The Lancet* **i**, 108-110.

Murphy, P. and Hill, R. E. (1991). Expression of the mouse *labial*-like homeobox-containing genes, *Hox-2.9* and *Hox-1.6*, during segmentation of the hindbrain. *Development* **111**, 61-74.

Noden, D. M. (1983). The role of the neural crest in patterning of avian cranial skeletal, connective and muscle tissues. *Dev. Biol.* **96**, 144-165.

Noden, D. M. (1988). Interaction and fates of avian craniofacial mesenchyme. *Development* **Supplement 103**, 121-140.

Otting, G., Qian, Y. Q., Billeter, M., Muller, M., Affolter, M., Gehring, W. J. and Wuthrich, K. (1990). Protein-DNA contacts in the structure of a homeodomain-DNA complex determined by nuclear magnetic resonance spectroscopy in solution. *EMBO J.* **9**, 3085-3092.

Pearse, A. G. E. and Carvalheira, A. F. (1967). Cytochemical evidence for an ultimobranchial origin of rodent thyroid C cells. *Nature* **214**, 929-930.

Pearse, A. G. E. and Polak, J. M. (1971). Cytochemical evidence for the neural crest origin of mammalian ultimobranchial C cells. *Histochemie* **27**, 96-102.

Pueblitz, S., Weinberg, A. G. and Albores-Saavedra, J. (1993). Thyroid C cells in the DiGeorge anomaly: a quantitative study. *Pediatr. Pathol.* **13 (4)**, 463-473.

Rijli, F. M., Mark, M., Lakkaraju, S., Dierich, A., Dollé, P. and Chambon, P. (1993). A homeotic transformation is generated in the rostral branchial region of the head by disruption of *Hoxa-2*, which acts as a selector gene. *Cell* **75**, 1333-1349.

Rogers, W. M. (1927). The fate of the ultimobranchial body in the white rat (Mus Norvegicus Albinus). *Am. J. Anat.* **38 (3)**, 349-477.

Rogers, W. M. (1971). Normal and anomalous development of the thyroid. In *The Thyroid* (ed. S. C. Werner and S. H. Ingbar) pp. 303-317. New York: Harper and Row.

Scott, M. P. (1992). Vertebrate homeobox gene nomenclature. *Cell* **71**, 551-553.

Serbedzija, G. N., Bronner-Fraser, M. and Fraser, S. (1992). Vital dye analysis of cranial neural crest cell migration in the mouse embryo. *Development* **116**, 297-307.

Sham, M. H., Hunt, P., Nonchev, S., Papalopulu, N., Graham, A., Boncinelli, E. and Krumlauf, R. (1992). Analysis of the murine *Hox-2.7* gene: conserved alternative transcripts with differential distributions in the nervous system and the potential for shared regulatory regions. *EMBO J.* **11**, 1825-1836.

Smith, D. B. and Johnson, K. S. (1988). Single-step purification of polypeptides expressed in *Escherichia coli* as fusions with glutathione S-transferase. *Gene* **67**, 31-40.

Swiatek, P. and Gridley, T. (1993). Perinatal lethality and defects in hindbrain development in mice homozygous for a targeted mutation of the zinc finger gene *Krox20*. *Genes Dev.* **7**, 2071-2084.

Tan, D.-P., Ferrante, J., Nazarali, A., Shao, X., Kozak, C. A., Guo, V. and Nirenberg, M. (1992). Murine *Hox-1.11* homeobox gene structure and expression. *Proc. Natl. Acad. Sci. USA* **89**, 6280-6284.

Wall, N. A., Jones, C. M., Hogan, B. L. M. and Wright, C. V. E. (1992). Expression and modification of *Hox-2.1* protein in mouse embryos. *Mech. Dev.* **37**, 111-120.

Wallin, J., Wilting, J., Koseki, H., Fritsch, R., Christ, B. and Balling, R. (1994). The role of *Pax-1* in axial skeleton development. *Development* **120**, 1109-1121.

Wilkinson, D. G., Bhatt, S., Cook, M., Boncinelli, E. and Krumlauf, R. (1989). Segmental expression of *Hox-2* homeobox-containing genes in the developing mouse hindbrain. *Nature* **341**, 405-409.

Wilkinson, D. G., Peters, G., Dickson, C. and McMahon, A. P. (1988). Expression of the FGF-related proto-oncogene *int-2* during gastrulation and neurulation in the mouse. *EMBO J.* **7**, 691-695.

Williams, E. D., Toyn, C. E. and Harach, H. R. (1989). The ultimobranchial gland and congenital thyroid abnormalities in man. *J. Pathol.* **159**, 135-141.

(Accepted 10 April 1995)